THE JOURNAL OF PHYSICAL CHEMISTRY B

Article

pubs.acs.org/JPCB

Molecular Dynamics Simulations of the Surface Tension and Structure of Salt Solutions and Clusters

Lu Sun,[†] Xin Li,[†] Thomas Hede,[‡] Yaoquan Tu,[†] Caroline Leck,[‡] and Hans Ågren*,[†]

[†]Department of Theoretical Chemistry and Biology, School of Biotechnology, Royal Institute of Technology, S-10691 Stockholm, Sweden

[‡]Department of Meteorology, Stockholm University, S-10691Stockholm, Sweden

ABSTRACT: Sodium halides, which are abundant in sea salt aerosols, affect the optical properties of aerosols and are active in heterogeneous reactions that cause ozone depletion and acid rain problems. Interfacial properties, including surface tension and halide anion distributions, are crucial issues in the study of the aerosols. We present results from molecular dynamics simulations of water solutions and clusters containing sodium halides with the interatomic interactions described by a conventional force field. The simulations reproduce experimental observations that sodium halides increase the surface tension with respect to pure water and that iodide anions reach the outermost layer of water clusters or solutions. It is found that the van der Waals interactions have an impact on the distribution of the halide anions and that a conventional force field with optimized parameters can model the surface tension of the salt solutions with reasonable accuracy.

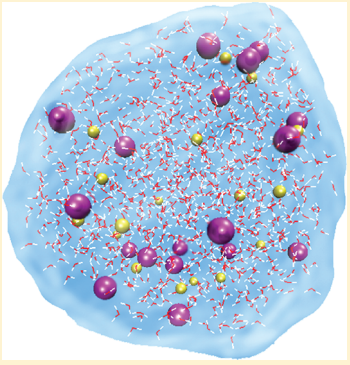

1. INTRODUCTION

Because the major part of planet Earth is covered with oceans, the interaction between the oceans in the marine regions and the atmosphere is of great importance. The oceans contain sea salt at approximately 3.5%, and this salt may be transferred to the troposphere.[1] Sea salt particles are found in marine aerosols and clouds, and studies of particle production in the atmosphere by bubbles bursting on the ocean have become the most often quoted.[2,3] They show two distinct methods of particle formation. One is from fragments of the bubble membrane (film) that are thrown into the air when the bubble bursts (film drops). The other is from drops of water that are detached from an upward-moving jet of water that follows the bubble burst (jet drops). It has generally been assumed that particles derived from film drops (100−500 nm in diameter) would be composed of sea salt (predominately sodium (Na^+) and chloride (Cl^-) ions but also of traces of other halides such as NaF (fluoride), NaBr (bromide), and NaI (iodide)). Sea salt has been found to contribute a significant fraction of the marine cloud condensation nucleus, CCN, population[4,5] and can thus through uptake of water vapor promote cloud formation[6] in the marine boundary layer. It is known that halide salts increase the surface tension of aqueous solutions, such as cloud droplets, with increasing concentration, influencing the water vapor condensation and therefore the cloud droplet growth, which in turn affects the optical properties of atmospheric aerosol particles and clouds and, in the end, even the precipitation mechanism.[7−10]

The cycle of sodium halides in the marine regions through the atmosphere and oceans is subject to feedback processes. In discussing climate feedback processes valid over the remote oceans, the so-called CLAW hypothesis[11] is commonly referred to. The CLAW hypothesis states that an increase in solar radiation stimulates the growth of phytoplankton in the oceans, which in turn generates dimethyl sulfide (DMS) as a breakdown product. DMS is converted into sulfate aerosol particles, which act as a CCN, and thus, more clouds and more reflective clouds form, decreasing the incoming solar radiation. This type of self-regulating feedback process has been embraced by the Gaia principle.[12] The belief that sea salt particles were few in numbers, too large, and found closest to the ocean surface lingered for a period of time after the presentation of the CLAW hypothesis, suggesting that sea salt particles do not affect the negative climate feedback process. However, Smith has shown that these assumptions are false, giving sea salt particles a more important role in the cloud formation in marine areas.[13] Sea salt particles are also the major chemical sink for sulfur dioxide (SO_2) in the cloudy marine boundary layer, hence affecting the CLAW hypothesis.

One other area of importance of sodium halides concerns heterogeneous reactions occurring on the surface of atmospheric aerosol particles generating, for example, the active halogen radicals responsible for polar ozone depletion and acid rain.[1,14−16] Sea salt in mixtures with organic compounds has been shown to have a joint effect on surface tension, increasing for low concentrations of surfactant and decreasing for higher concentrations,[17] thereby affecting the uptake of water vapor.

Solutions containing sodium halides have been extensively studied both theoretically and experimentally.[18−25] Molecular dynamics (MD) simulations of the solution/air interfaces have

Received: September 22, 2011
Revised: January 23, 2012
Published: February 21, 2012

been reported on several occaisons.[18,19] These studies reveal that iodide anions tend to reside on the surface while fluoride anions are repelled from the surface.[18−22] Further experiments have confirmed that iodide and bromide anions do reach the ion/water interface.[23−25] This interface phenomenon has attracted much attention in recent years, and the most common explanation is that the difference of anion distributions is mainly due to the polarization effect.[18,19,26−28]

To build beyond previous MD simulation studies, this study makes an attempt to elucidate the role of sodium halides and their effects on the aerosol, especially surface tension. Solution simulations employing a conventional nonpolarizable force field with optimized parameters for the ions to model the potentials were carried out as a comparison to the similar systems reported by Jungwirth et al.[18] Some large water clusters, containing 1000 or 2000 water molecules and sodium halides, were studied

2. COMPUTATIONAL METHODS

2.1. Solutions. MD simulations were performed with the Gromacs program package.[29−32] The solution/air interfaces of the salt solutions were modeled by water slabs with the sodium halide concentration of 1.2 M. Several systems, each consisting of 864 water molecules as well as 18 Na^+ and 18 X^- (X^- = F^-, Cl^-, Br^-, or I^-) ions, were evaluated. A pure water system of 864 water molecules was also modeled as the control. Each system was in the center of a rectangular box with a size of 100 × 100 × 30 Å^3, and the period boundary condition (PBC) was applied. The Lennard-Jones potential was used, and parameters for ions were taken from the OPLS/AA force field.[33] The semiflexible SPC/E water model[34] was used with the OH bond length constrained at 1.0 Å by the LINCS algorithm[35,36] during the simulations. The H−O−H bond angle in the water molecule was set to be flexible and modeled by a harmonic potential with an equilibrium angle of 109.47° and a force constant of 383.0 kJ mol^{-1} rad^{-2}.[34] The Lennard-Jones parameters used in this work are listed in Table 1. The *NVT* ensemble was employed with the temperature maintained at 300 K by the Nosé−Hoover thermostat.[37,38] The cutoff distances for the Coulombic and van der Waals interactions were set to 1.2 nm. The particle mesh Ewald summation method[39,40] was applied to compute the long-range Coulombic interactions.

Table 1. Lennard-Jones Parameters of Ions[a]

	σ (nm)	ε (kJ mol^{-1})
Na^+	0.333045	0.011598
F^-	0.273295	3.012480
Cl^-	0.441724	0.492833
Br^-	0.462376	0.376560
I^-	0.540000	0.292880

[a]The Lennard-Jones potential is expressed as $V_{LJ} = 4\varepsilon[(\sigma/r)^{12} - (\sigma/r)^6]$.

For each system, the simulation was carried out with a time step of 1 fs and a total simulation time of 6 ns, comprised of 1 ns for equilibration and 5 ns for data analysis. The surface tension and distributions of ions were obtained by analyzing the trajectories recorded at every 500 fs.

The surface tension of a planar system is normally a combination of the origin part γ_o and the dispersion part γ_d. Taking advantage of the diagonal components of the pressure tensor (P_{zz},P_{xx},P_{yy}) and the box length along the z-axis (L_z), we can calculate the origin part as[41]

$$\gamma_o = \frac{1}{2}L_z\left[P_{zz} - \frac{1}{2}(P_{xx} + P_{yy})\right] \quad (1)$$

Because the Lennard-Jones potential is truncated at the cutoff in the simulations, estimation of the dispersion correction is needed to fit the number density along the z-axis to the hyperbolic tangent function

$$\rho(z) = \frac{1}{2}(\rho_\alpha + \rho_\beta) - \frac{1}{2}(\rho_\alpha - \rho_\beta)\tanh\left(\frac{z - z_0}{\xi}\right) \quad (2)$$

where ρ_α is the liquid-phase density and ρ_β is the gas-phase density. The dispersion correction is obtained as

$$\begin{aligned}\gamma_d &= 12\pi\varepsilon\sigma^6(\rho_L - \rho_V)^2\int_0^1 ds\int_{r_c}^{\infty} dr\,(3s^3 - s)r^{-3}\coth\left(\frac{rs}{\xi}\right)\\ &= 12\pi\varepsilon\sigma^6(\rho_L - \rho_V)^2\int_0^1 ds\int_0^{1/r_c} dr'\,(3s^3 - s)r'\coth\left(\frac{s}{\xi r'}\right)\end{aligned} \quad (3)$$

where we apply the substitution $r' = r^3$ so as to acquire double integration on finite intervals. An average value of $\varepsilon\sigma^6$ is used for multicomponent systems

$$\langle\varepsilon\sigma^6\rangle = \frac{2}{N(N-1)}\sum_{i=1}^{N}\sum_{j>i}^{N}\varepsilon_{ij}\sigma_{ij}^6 \quad (4)$$

2.2. Clusters. Clusters of 1000 and 2000 water molecules were constructed, and the concentrations of sodium halides in the clusters were controlled at 1 M by inserting 18 Na^+ and 18 X^- (X^- = F^-, Cl^-, Br^-, or I^-) ions into the cluster of 1000 water molecules or 36 Na^+ and 36 X^- ions into that of 2000 water molecules. In addition, two pure water clusters, with 1000 and 2000 water molecules, were considered for comparison. Each cluster was placed into the middle of a cubic box with the side length of 6 nm larger than the diameter of the cluster to mimic the droplet and minimize the interactions of the cluster with its images because the PBC was adopted. The OPLS/AA force field in combination with semiflexible the SPC/E water model was also applied, and the modeling temperature was maintained at 298 K to achieve the atmospheric environment. The van der Waals interactions were truncated at 1.5 nm. Each simulation was carried out with a time step of 1 fs and a total simulation time of 8 ns, comprised of 3 ns for equilibration and 5 ns for data analysis.

The surface tension of an isolated spherical droplet can be estimated from the work of formation and the radius for an equimolar surface, according to the formula by Thompson et al.[42] The normal component of the Ivring−Kirkwood pressure tensor, $P_N(r)$, which consists of kinetic and configuration terms, is calculated from the trajectory files, as shown below[43]

$$P_N(r) = P_K(r) + P_U(r) = k_B T\rho(r) + S^{-1}\sum_k f_k \quad (5)$$

dx.doi.org/10.1021/jp209178s | J. Phys. Chem. B 2012, 116, 3198−3204

where k_B is the Boltzmann constant, T is the temperature of the system, S is the surface area of the sphere with radius r, and f_k is the component of the pairwise force orthogonal to the surface.

The work of formation can be derived from the obtained P_N as[44]

$$W = 2\pi \int_0^{R_\beta} P_N(r) r^2 \, dr - 2\pi P^\beta R_\beta^3/3 \quad (6)$$

where P^β is the vapor pressure and R_β is a radius in the vapor region where $P_N(r)$ equals P^β.

From density profiles, the equimolar surface radius R_e is calculated as

$$R_e^3 = -\frac{1}{\rho_\alpha - \rho_\beta} \int_0^\infty r^3 \frac{d\rho(r)}{dr} dr \quad (7)$$

Here, ρ_α and ρ_β are the densities of the liquid and vapor, respectively. Finally, the surface tension is evaluated as

$$\gamma \approx \gamma_e = \frac{3W}{4\pi R_e^2} \quad (8)$$

3. RESULTS AND DISCUSSION

3.1. Solutions. The surface tension of each solution was computed based on the modeling of the corresponding slab system and is compared with the experimental data in Table 2.

Table 2. Surface Tension of Water Solutions with Sodium Halides[a]

		$\Delta\gamma$ (mJ/m^2)	
solution	γ (mJ/m^2)	simulation	experiment[45,46]
NaF	67.5	3.1	3.6
NaCl	67.0	2.6	2.0
NaBr	66.4	2.0	1.6
NaI	65.9	1.5	1.2
H_2O	64.4		

[a] γ is the surface tension calculated from eqs 1−4. $\Delta\gamma$ is the increase of the surface tension with respect to pure water. The experimental data are obtained by extrapolation and interpolation of values in refs 45 and 46 because temperature influence is negligible and the surface tension shifts linearly over a wide range of sodium halide concentrations.

Even though the force field that we employed is nonpolarizable, the slight increase of the surface tension of the solutions with respect to that of the pure water system as well as the order of the increase of the surface tension, $I^- < Br^- < Cl^- < F^-$, is obtained in accordance with the experimental observation. Compared with the experimental data, our calculations for solutions of NaCl, NaBr, or NaI, slightly overestimate the increase of the surface tension, while for the NaF solution, the increase of the surface tension is slightly underestimated. As a result, the difference of the surface tensions between NaF and NaCl solutions is only 0.5 mJ/m^2, smaller than the corresponding experimental value (1.6 mJ/m^2). That the Lennard-Jones parameters for the F^- ion is not so appropriate for the calculation of the surface tension of NaF solutions is probably attributed to the smaller σ value and the far larger ε value in terms of the Lennard-Jones parameters for other halogen ions, displayed in Table 1. Despite the fact that a nonpolarizable potential is used to describe the water−ion and ion−ion interactions, the Lennard-Jones parameters for the ions are generally optimized for the simulation of such systems because the surface tension values achieved are closer to those from experiment than from the classical polarizable model.[18]

3.1.2. Anion Distribution. The increase of the surface tension of the solutions with sodium halide is closely related to the anion distributions in the solutions, which have been studied both theoretically and experimentally. The distributions of anions in the solutions are illustrated in Figure 1. Except for F^-, the halide anions are closer to the surface than the Na^+ ions, consistent with the previous study.[18] Apparently, the F^- anions are most devoid on the surface. The distribution of Cl^- anions is rather similar to that of Br^- anions, and both are repelled from the surface. The distribution of Br^- anions seems to be in disagreement with simulations with a polarizable potential or experimental results where Br^- anions reached the interface.[18,23] The I^- anions are found to be abundant near the interface, whereas the outermost peak of the I^- distribution is not so outward as the results obtained by Jungwirth et al.[18] Nevertheless, their classical polarizable potential model probably overestimated the polarization effect because such a high concentration of I^- anions on the surface was not observed experimentally either.[21,23,26] Recently, Levin et al.[26] claimed that the ion distribution was dominated by hydration and that heavy halide anions, such as Br^- and I^-, are not hydrated, but the large polarization effect makes these ions reside on the surface. Moreover, Caleman et al. calculated the free energy of each composition of the cluster system with single halide anion and demonstrated that the unique halide anion distribution was caused by the joint effect of charge, size, polarization of anions and water, and so on.[47] Because the polarization effect of ions is not taken into account in our simulations, the difference in anion distributions is totally induced by the difference in the Lennard-Jones parameters for the ions representing the van der Waals interaction. We can draw a conclusion that the Lennard-Jones parameters used in the potential model will dramatically affect the ion distributions, and therefore, the van der Waals interaction is also a dominant factor for the ion distribution.

3.2.1. Clusters. *Cutoff Radius.* The accuracy of MD simulations depends significantly on the cutoff concerning nonbonded interactions. In particular, we have found that the surface tension of a cluster is sensitive to the cutoff radius used in the simulations. Usually, results are more accurate with a larger cutoff radius because more pairwise interactions are taken into account. In order to find a reasonable cutoff for the simulation of the water clusters with sodium halides, we tested different cutoffs for a cluster of 2000 water molecules with 36 Na^+ and 36 Cl^- ions to measure how its surface tension changes with the cutoff used in the simulations; the results are shown in Figure 2. Due to the fact that more pairwise van der Waals interactions are accounted for and thus a more accurate structure of the cluster is generated with the increase of the cutoff, the surface tension increases dramatically when the cutoff radius varies from 1.0 to 1.2 nm. After the cutoff reaches 1.2 nm, the surface tension value rises a little and fluctuates around a certain value. The relation between the surface tension and the cutoff can be fitted by a function $\gamma = a - b \times c^{\gamma_c}$, with $a = 107.14$, $b = 2.35$, and $c = 7.7 \times 10^{-6}$ (γ denotes surface tension, while γ_c represents the cutoff radius). As seen in Figure 2, the surface tension is closest to the convergence value when the cutoff reaches 1.5 nm among the six systems that we modeled. This means that beyond this cutoff, the van der Waals interaction has a minor effect on the cluster structure. Therefore, the cutoff value for the nonbonded

dx.doi.org/10.1021/jp209178s | J. Phys. Chem. B 2012, 116, 3198−3204

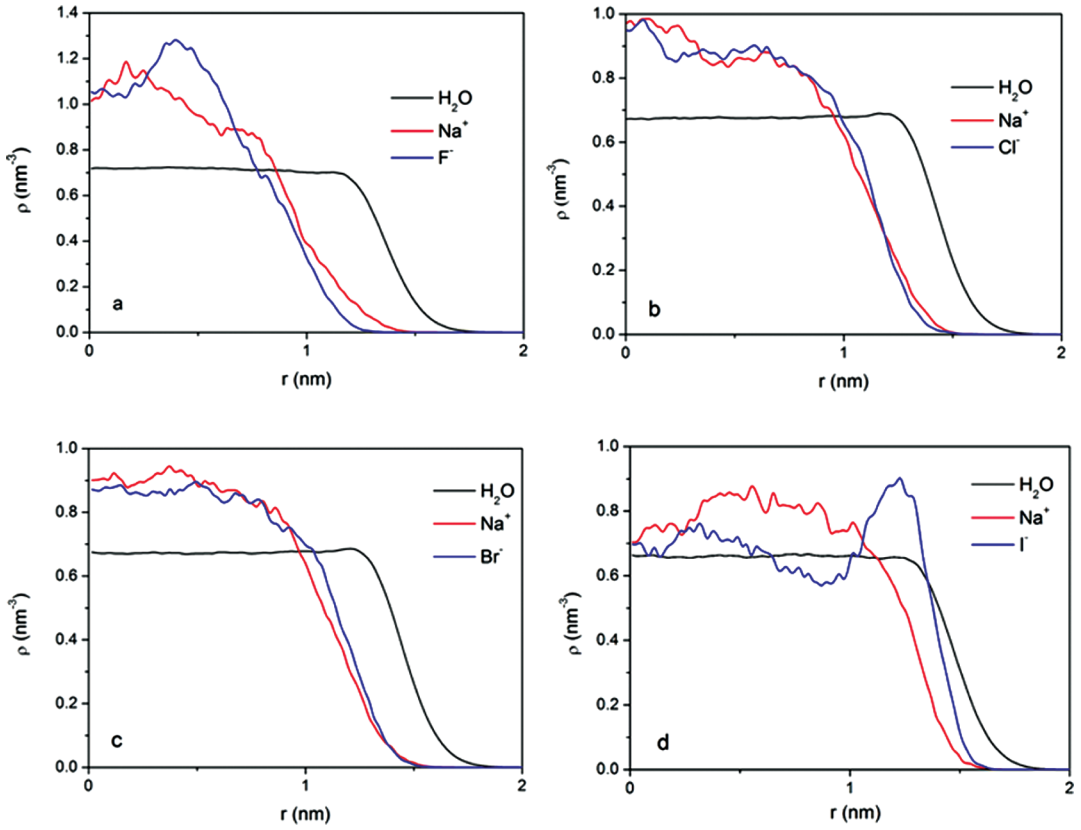

Figure 1. Radial number densities (ρ) of water and ions for different slab systems; r denotes the distance to the center of mass. (a) 864 H_2O + 18 NaF, (b) 864 H_2O + 18 NaCl, (c) 864 H_2O + 18 NaBr, and (d) 864 H_2O + 18 NaI.

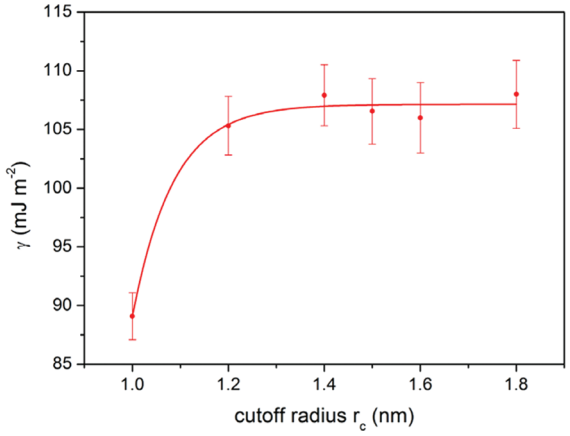

Figure 2. Change of the surface tension (γ) of the NaCl cluster with the cutoff radius (γ_c). The cluster is of 2000 water molecules with 36 Na^+ and 36 Cl^- ions.

interaction is set to 1.5 nm in all of our simulations of the clusters to minimize error caused by the structure. This cutoff is larger than the often used cutoffs (~0.8−1.2 nm) in simulations.

3.2.2. Surface Tension. The calculated surface tension, together with other properties, such as the number density, the equimolar surface radius, and the work of formation, for all of the clusters is listed in Table 3.

When sodium halide is added to the pure water cluster, the surface tension of the resulting clusters increases in the order $F^- > Cl^- > Br^- > I^-$, which coincides with the slab systems. This order is related to the distribution of the anions discussed later. The densities for the two pure water clusters are larger than the density of pure bulk water from our simulation with a semiflexible SPC/E water model (33.669 nm^{-3}), reflecting that the clusters are more compressed than slabs. The densities of the clusters with iodide anions are smaller than those for the corresponding pure water clusters, and their equimolar surface radii are the largest compared with the other clusters with the same number of water molecules.

It is worthwhile to notice that the enhancement of the surface tension induced by iodide anions is not so dramatic, about 2 mJ/m^2 for the clusters of 1000 and 2000 water molecules. This observation can be explained based on the peak of the iodide system in Figure 3, where the iodide anions make the clusters less compressed due to their peculiar distribution that iodide anions are abundant near the surface.

Table 3. Calculated Number Density (ρ), Equimolar Surface Radius (R_e), Work of Formation (W), and Surface Tension (γ)

system	ρ (nm^{-3})	R_e (nm)	W (10^{-19} J)	γ (mJ/m^2)
1000 H_2O	34.727	1.90	11.19	73.87
1000 H_2O + 18 NaF	37.955	1.87	14.00	95.67
1000 H_2O + 18 NaCl	35.247	1.91	14.44	94.55
1000 H_2O + 18 NaBr	35.157	1.92	13.96	90.77
1000 H_2O + 18 NaI	34.298	1.93	11.89	76.08
2000 H_2O	34.554	2.40	20.13	83.48
2000 H_2O + 36 NaF	37.521	2.36	25.46	108.96
2000 H_2O + 36 NaCl	34.976	2.42	26.12	106.55
2000 H_2O + 36 NaBr	34.916	2.42	24.05	98.07
2000 H_2O + 36 NaI	34.038	2.44	21.36	85.63

dx.doi.org/10.1021/jp209178s | J. Phys. Chem. B 2012, 116, 3198−3204

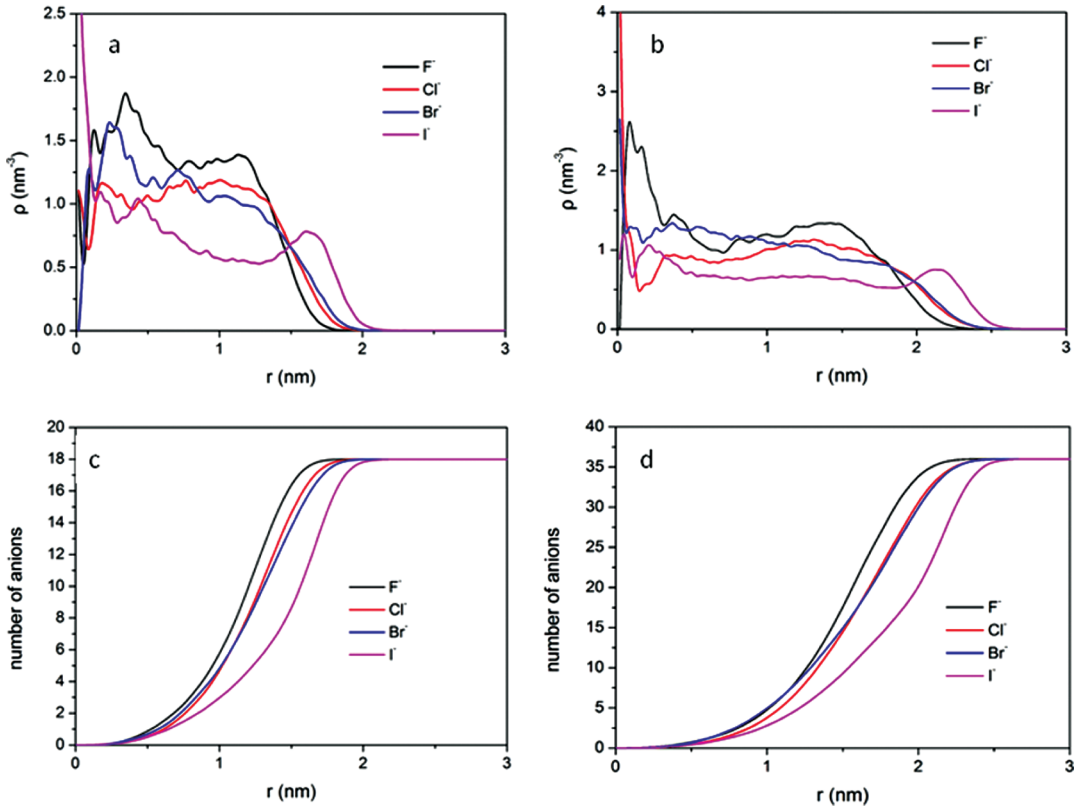

Figure 3. Radial number densities (ρ) and integrations of distributions of halide anions in 1000 and 2000 H_2O systems. (a) Radial number densities of anions in clusters of 1000 H_2O with 18 sodium halide, (b) radial number densities of anions in clusters of 2000 H_2O with 36 sodium halide, (c) integrations of number densities in clusters of 1000 H_2O, and (d) integrations of number densities in clusters of 2000 H_2O.

The shorter van der Waals radius makes the clusters with fluoride anions more compressed and results in larger number densities of the fluoride anions inside the clusters. The differences of the number densities and the equimolar surface radii of the clusters with those of other systems are evident. Work of formation, number density, and equimolar surface radius are dominating factors in the description of the surface tension. Although the work of formation for the clusters with fluoride anions is smaller than that for the corresponding cluster with chloride anions, the larger number density and the smaller equimolar surface radius makes the cluster with fluoride anions acquire larger surface tension. From Figure 3, we can also find that the surface tension increases about 10 mJ/m^2 when the cluster size is increased from 1000 water molecules to 2000 water molecules.

3.2.3. Distributions of Anions. Distributions and their integrations of anions are studied from trajectories and presented in Figure 3. The radial number density of iodide anions has a peak at the outermost layer. Peaks of other anions move inward. The peak of fluoride anions is most repelled from the interface. These characteristics are in accord with our study of solutions with sodium halides. Moreover, from the integration of the radial number density, it is worth noticing that the number of fluoride anions rises fastest with the increase of the distance from the center of a cluster to its surface (r), implying that, compared with the other halide ions, fluoride anions are distributed away from the surface. The number of iodide anions increases slowest with the increase of r, indicating that more iodide anions reside nearer to the surface compared with the clusters with other halide ions.

3.2.4. Normal Component of the Ivring–Kirkwood Pressure Tensor. Because the surface tension is calculated based on the work of formation and the equimolar surface radius, the normal component of the Ivring–Kirkwood pressure tensor, $P_N(r)$, which dominates the work of formation, is of interest. The $P_N(r)$ profile of each system is computed and shown in Figure 4.

As illustrated in Figure 4, the $P_N(r)$ profiles for systems of 1000 and 2000 water molecules are similar in the way that all curves show a peak near the surface. $P_N(r)$ profiles for clusters with fluoride anions have the highest and most inward peaks, while those for clusters with iodide anions show the lowest and outermost peaks. This observation could be correlated with the van der Waals interactions related to the halogen ions. Of the anions studied, the fluoride anion has the smallest σ value and largest ε value, and thus, it has the strongest van der Waals interaction with other ions and water molecules. In contrast, the iodide anion has the largest σ value and smallest ε value, and it therefore has the weakest van der Waals interaction with other ions and water molecules.

4. CONCLUSION

Water slabs and clusters with sodium halides were simulated in order to explore the technical requirements of molecular dynamics simulations to treat these sea salt aerosols both as prototypes and as benchmarks for more complex clusters of atmospheric relevance. Radial number densities of different anions were evaluated, and the surface tension was computed. The OPLS/AA force field for ions is found to be appropriate for describing the surface tension and the ion–ion and ion–water interactions in the water slab systems. It is found that the

dx.doi.org/10.1021/jp209178s | J. Phys. Chem. B 2012, 116, 3198–3204

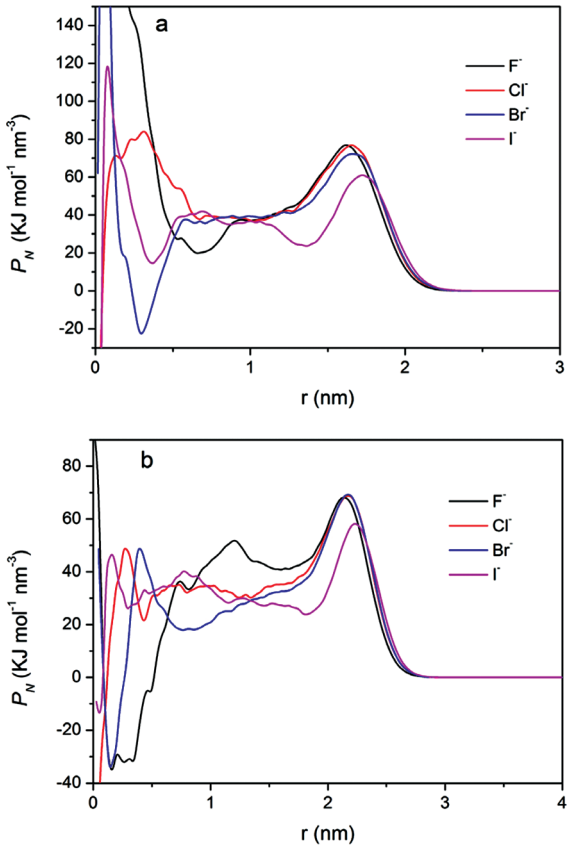

Figure 4. Normal component of the Ivring–Kirkwood pressure tensor $P_N(r)$. (a) Clusters of 1000 water molecules and (b) Clusters of 2000 water molecules.

surface tension converges when the cutoff for nonbond interaction in clusters goes beyond about 1.4 nm. The anion distributions in a cluster and in the corresponding slab system are similar. Of the halide anions studied, iodide anions present the largest number density close to the interface, while fluoride anions are repelled the most from the interface. Clusters with fluoride anions exhibit the largest surface tension, while clusters with iodide anions showed the smallest. The van der Waals interaction is proven to be a crucial factor for the anion distributions. MD simulations employing a nonpolarizable force field with optimized parameters can accurately model the surface tension and other properties of water with halide ions. This finding has practical ramifications as a nonpolarizable force field greatly saves computational cost, in particular, for the simulation of large clusters. We find that the significant influence rendered by van der Waals interaction as well as other results from this work provides important know-how when we now embark on more complex clusters of atmospheric relevance such as mixed amino acid sea salt aerosols abundant over marine areas.

AUTHOR INFORMATION

Corresponding Author

*Address: Department of Theoretical Chemistry, Royal Institute of Technology, Roslagstullsbacken 15, S-106 91 Stockholm, Sweden. Phone: +46-85537 8416. Fax: +46-855378590. E-mail: agren@theochem.kth.se.

Notes

The authors declare no competing financial interest.

ACKNOWLEDGMENTS

The authors thank the Swedish National Infrastructure Committee (SNIC) for providing computational resources for the project "Multi-physics Modeling of Molecular Materials", SNIC022/09-25. H.A. acknowledges support from the Swedish Science Research Council (VR, Ccontract 2009-3614).

REFERENCES

(1) Ravishankara, A. R. *Science* **1997**, *276*, 1058–1065.
(2) Blanchard, D. C.; Woodcoak, A. H. *Tellus* **1957**, *9*, 145–158.
(3) Blanchard, D. C. *The electrification of the atmosphere by particals from bubbles in the sea*; Pergamon Press: New York, 1963; Vol. *I*.
(4) O'Dowd, C. D.; Smith, M. H. *J. Geophys. Res.* **1993**, *98*, 1137–1149.
(5) O'Dowd, C. D.; Lowe, J. A.; Smith, M. H. *Geophys. Res. Lett.* **1999**, *26*, 1311–1314.
(6) Köhler, H. *Trans. Faraday Soc.* **1936**, *32*, 1152–1161.
(7) Ramanathan, V.; Cess, R. D.; Harrison, E. F.; Minnis, P.; Barkstrom, B. R.; Ahmad, E.; Hartmann, D. *Science* **1989**, *243*, 57–63.
(8) Li, X.; Hede, T.; Tu, T.; Leck; Ågren, H.; C.. *J. Phys. Chem. Lett.* **2010**, *1*, 769–773.
(9) Rodhe, H. *Nature* **1999**, *401*, 223–225.
(10) Charlson, R. J.; Seinfeld, J. H.; Nenes, A.; Kulmala, M.; Laaksonen, A.; Facchini, M. C. *Science* **2001**, *292*, 2025–2026.
(11) Charlson, R. J.; Lovelock, J. E.; Andreae, M. O.; Warren, S. G. *Nature* **1987**, *326*, 655–661.
(12) Lovelock, J. E. *Nature* **1990**, *344*, 100–102.
(13) Smith, M. H. *Environ. Chem.* **2007**, *4*, 391–395.
(14) Solomon, S.; Portmann, R. W.; Garcia, R. R.; Thomason, L. W.; Poole, L. R.; McCormick, M. P. *J. Geophys. Res.* **1996**, *101*, 6713–6727.
(15) Sievering, H.; Boatman, J.; Gorman, E.; Kim, Y.; Anderson, L.; Ennis, G.; Luria, M.; Pandis, S. *Nature* **1992**, *360*, 571–573.
(16) Vogt, R.; Crutzen, P. J.; Sander, R. *Nature* **1996**, *383*, 327–330.
(17) Tuckermann, R. *Atmos. Environ.* **2007**, *41*, 6265–6275.
(18) Jungwirth, P.; Tobias, D. J. *J. Phys. Chem. B* **2001**, *105*, 10468–10472.
(19) Jungwirth, P.; Tobias, D. J. *J. Phys. Chem. B* **2002**, *106*, 6361–6373.
(20) Chang, T.; Dang, L. X. *Chem. Rev.* **2006**, *106*, 1305–1322.
(21) Guàrdia, E.; Skarmoutsos, I. *J. Chem. Theory. Comput.* **2009**, *5*, 1449–1453.
(22) Jungwirth, P.; Tobias, D. J. *Chem. Rev.* **2006**, *106*, 1259–1281.
(23) Ghosal, S.; Hemminger, J. C.; Bluhm, H.; Mun, B. S.; Hebenstreit, E. L. D.; Ketteler, G.; Ogletree, D. F.; Requejo, F. G.; Salmeron, M. *Science* **2005**, *307*, 563–566.
(24) Petersen, P. B.; Saykally, R. J. *J. Phys. Chem. B* **2005**, *109*, 7976–7980.
(25) Petersen, P. B.; Saykally, R. J. *J. Am. Chem. Soc.* **2005**, *127*, 15446–15452.
(26) Baer, M. D.; Mundy, C. J. *J. Phys. Chem. Lett.* **2011**, *2*, 1088–1093.
(27) Levin, Y.; dosSantos, A. P.; Diehl, A. *Phys. Rev. Lett.* **2009**, *103*, 257802–257805.
(28) Levin, Y. *Phys. Rev. Lett.* **2009**, *102*, 147803–147806.
(29) Hess, B.; Kutzner, C.; van der Spoel, D.; Lindahl, E. *J. Chem. Theory. Comput.* **2008**, *4*, 435–447.
(30) van der Spoel, D.; Lindahl, E.; Hess, B.; Groenhof, G.; Mark, A. E.; Berendsen, H. J. C. *J. Comput. Chem.* **2005**, *26*, 1701–1719.
(31) Lindahl, E.; Hess, B.; van der Spoel, D. *J. Mol. Model.* **2001**, *7*, 306–317.
(32) Berendsen, H. J. C.; van der Spoel, D.; van Drunen, R. *Comput. Phys. Commun.* **1995**, *91*, 43–56.
(33) Jorgensen, W. L.; Maxwell, D. S.; Tirado-Rives, J. *J. Am. Chem. Soc.* **1996**, *118*, 11225–11236.
(34) Berendsen, H. J. C.; Grigera, J. R.; Straatsma, T. P. *J. Phys. Chem.* **1987**, *91*, 6269–6271.

(35) Hess, B.; Bekker, H.; Berendsen, H. J. C.; Fraaije, J. G. E. M. *J. Comput. Chem.* **1997**, *18*, 1463−1472.
(36) Hess, B. *J. Chem. Theory. Comput.* **2007**, *4*, 116−122.
(37) Nosé, S. *Mol. Phys.* **1984**, *52*, 255−268.
(38) Hoover, W. G. *Phys. Rev. A* **1985**, *31*, 1695−1697.
(39) Darden, T.; York, D.; Pedersen, L. *J. Chem. Phys.* **1993**, *98*, 10089−10092.
(40) Essmann, U.; Perera, L.; Berkowitz, M. L.; Darden, T.; Lee, H.; Pedersen, L. G. *J. Chem. Phys.* **1995**, *103*, 8577−8592.
(41) Alejandre, J.; Tildesley, D. J.; Chapela, G. A. *J. Chem. Phys.* **1995**, *102*, 4574−4583.
(42) Thompson, S. M.; Gubbins, K. E.; Walton, J. P. R. B.; Chantry, R. A. R.; Rowlinson, J. S. *J. Chem. Phys.* **1984**, *81*, 530−542.
(43) Irving, J. H.; Kirkwood, J. G. *J. Chem. Phys.* **1950**, *18*, 817−829.
(44) Zakharov, V. V.; Brodskaya, E. N.; Laaksonen, A. *J. Chem. Phys.* **1997**, *107*, 10675−10683.
(45) Hey, M. J.; Shield, D. W.; Speight, J. M.; Will, M. C. *J. Chem. Soc.* **1981**, *77*, 123−128.
(46) Washburn, E. W. *International Critical Tables of Numerical Data, Physics, Chemistry, and Technology*; McGraw-Hill: New York, 1928; Vol *IV*.
(47) Caleman, C.; Hub, J. S.; van Maaren, P. J.; van der Spoel, D. *Proc. Natl. Acad. Sci. U.S.A.* **2011**, *108*, 6838−6842.